Cloaking a circular cylinder in deep water

J. N. Newman
jnn@mit.edu

(Submitted to 28th IWWWFB – L'Isle sur la Sorgue, France – 7-10 April 2013)

1 Introduction

In the diffraction problem, where a fixed body scatters the incident waves, 'cloaking' refers to the condition where there is no scattering in the form of radial outgoing waves. The possibility of cloaking in the diffraction of water waves is of scientific interest, since it is not obvious that this condition can be achieved with a body of nonzero volume on or near the free surface. Cloaking may also have practical applications, such as reducing the mean drift force.

Porter [1] and Newman [2] have considered the possibility of cloaking a bottom-mounted circular cylinder, using an annular bed with variable depth in both the radial and azimuthal directions. Their computations show that near-zero values of the scattered energy can be achieved by optimizing the bathymetry of the bed. Subsequently, in response to a stimulating question at the last Workshop [3], axisymmetric beds have been discovered with equally small values of the scattered energy [4]. This surprising discovery contradicts the author's conjecture in the reply to [3].

The use of variable bathymetry may be impractical, especially in deep water. Thus the present work considers the possibility of cloaking a circular cylinder of finite draft in a fluid of infinite depth. Two types of surrounding structures are used to minimize the total scattered energy. The first is an array of smaller cylinders which surround the inner cylinder, as shown in Figure 1. This configuration was suggested by the work of Farhat et al [5]. The second type is an axisymmetric ring (toroid) with the cross-section represented by a Fourier series. In both cases it is shown that the scattered energy can be reduced to very small values by optimizing the dimensions and shape of the surrounding bodies.

As in [2], the approach is based on minimizing the scattered energy computed by WAMIT, using multi-variate optimization to search for the appropriate values of the geometrical parameters. The results are normalized based on unit values of the incident-wave amplitude, fluid density, and draft of the inner cylinder. The radius of the inner cylinder is 0.5 and the optimizations are performed at the wavenumber $K = 1$. The scattered energy is computed from the Kochin function, which represents the amplitude of the far-field radiating waves, using equation 7 of [2].

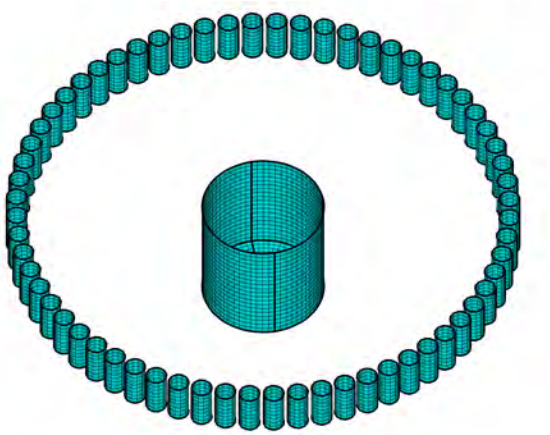

Figure 1: Perspective view of the optimized structure with $N = 64$ outer cylinders.

2 Arrays of circular cylinders

N circular cylinders with radius r and draft d are uniformly spaced around a circle of radius R_0, concentric with the inner cylinder. The entire structure is fixed on the free surface. Five different arrays are considered with N=(4,8,16,32,64), as shown in Figure 2. The incident waves propagate in the direction parallel to the horizontal axis in Figure 2. Optimum values of the parameters r, d and R_0 are computed to minimize the energy. Table 1 shows the values of these parameters with the corresponding minima of the scattered energy E and ratio E/E_0, where E_0 is the scattered energy of the inner cylinder by itself.

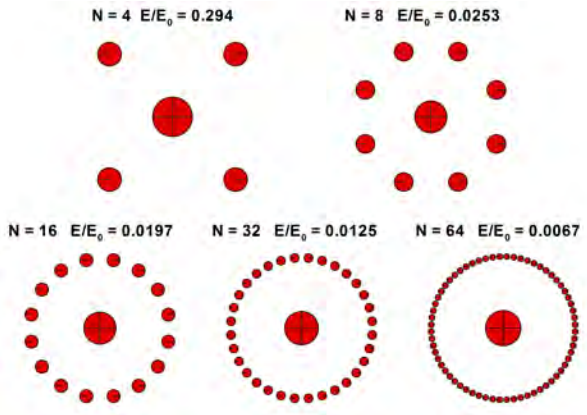

Figure 2: Plan view of the arrays N=4,8,16,32,64.

Figure 3 shows the scattered energy for a range of wavenumbers. The results for $N \geq 8$ are practically the same, with very small values at $K = 1$ and substantially less energy in the range $0.7 < K < 1.2$ compared to the inner cylinder by itself. From momentum conservation it follows that the mean drift force is small if the scattered energy is small. This is confirmed in Figure 4.

Since E decreases as N increases, and the array approximates an axisymmetric ring as $N \to \infty$, these results suggest the possibility of cloaking with an axisymmetric structure and motivate the alternative configuration in Section 3.

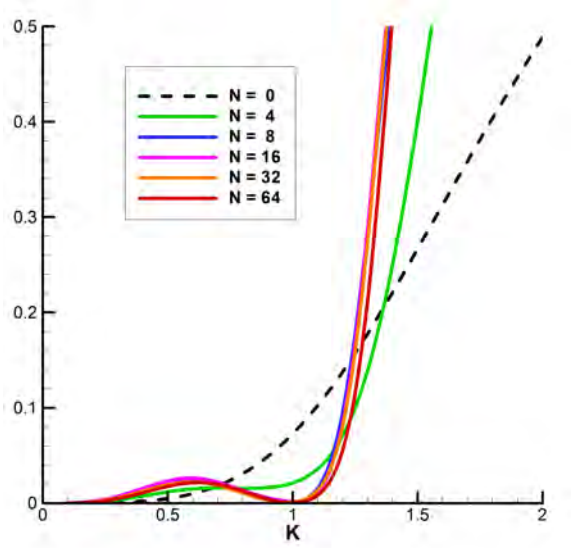

Figure 3: Scattered energy for the cylinder alone ($N = 0$) and five optimized structures shown in Figure 2.

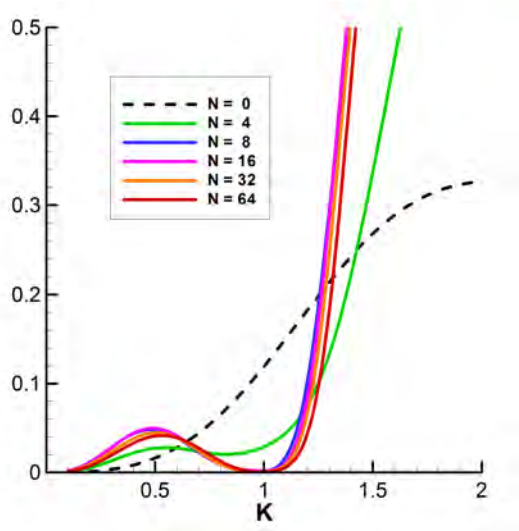

Figure 4: Mean drift force on the cylinder and five optimized structures.

N	r	d	R_0	E	E/E_0
4	0.2993	0.3434	2.2071	0.0214	0.2939
8	0.2933	0.4745	2.2031	0.0018	0.0253
16	0.1963	0.4785	2.1592	0.0014	0.0197
32	0.1309	0.4507	2.1003	0.0009	0.0125
64	0.0848	0.3606	2.0170	0.0005	0.0067

Table 1: Optimized parameters of the arrays.

3 Axisymmetric rings

In this configuration the surrounding structure is a toroid with its cross-section defined by

$$R = R_0 + \sum_{m=1}^{[(N-1)/2]} S_m \sin m\psi + \sum_{m=1}^{[(N-2)/2]} C_m \cos m\psi,$$

$$z = -d \cos \psi.$$

Here (R, z) are cylindrical coordinates with R the radius from the vertical $z-$axis, $z = 0$ the plane of the free surface and z positive upward. The parametric coordinate ψ varies between $-\pi/2$ on the inner waterline and $\pi/2$ on the outer waterline. The optimization parameters include R_0, d, and the Fourier coefficients S_m and C_m. In the simplest case $N = 3$ only S_1 is included and the cross-section is elliptical, as shown in Figure 5.

The minimum values of the energy ratio E/E_0 are shown in Figure 6 for $N \leq 16$. It is evident that ratios on the order of 10^{-4} represent the limit of what can be achieved using the single-precision code WAMIT. These values of the energy ratio are substantially smaller than the corresponding results in Section 2, providing numerical evidence

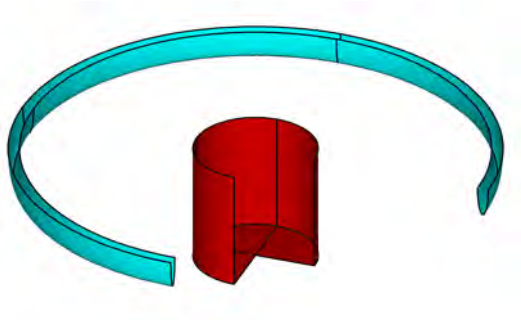

Figure 5: Perspective view of the cylinder and toroid with elliptical section (N=3). One quadrant is omitted to show the cross-section.

for the existence of axisymmetric cloaking structures. The optimized sections are shown in Figure 7. For $N \geq 12$ these are practically identical. The coefficients for $N \leq 8$ are listed in Table 2.

Figure 8 shows the mean drift force for the structure $N = 16$, including the separate components acting on the cylinder and toroid. It is interesting to note that both of these components have zero-crossings at $K = 1$. Thus the occurrence of near-zero mean drift force on the complete structure is not a consequence of cancellation between the two components. This is explained below.

If the incident-wave potential is the product of a real function and e^{-ikx}, the symmetric and anti-symmetric components of the scattered potential satisfy Neumann boundary conditions on the body where the normal derivatives are real and imaginary, respectively. If there is no scattered energy these potentials vanish at infinity faster than a radiated wave, and satisfy homogeneous boundary conditions on the free surface (and bottom). It follows that they are respectively real and imaginary throughout the fluid domain, assuming uniqueness. Thus there is no anti-symmetric component of the second-order mean pressure, and no drift force acting on sub-elements of the body which

	N= 3	4	5	6	7	8
R_0	1.926	1.656	1.654	1.481	1.466	1.450
d	0.241	0.245	0.258	0.253	0.252	0.259
S_1	0.046	0.054	0.051	0.058	0.060	0.060
C_1		-0.072	-0.074	-0.053	-0.056	-0.055
S_2			-0.014	-0.022	-0.024	-0.016
C_2				-0.039	-0.040	-0.036
S_3					0.002	-0.002
C_3						0.035

Table 2: Optimized parameters for toroids $N \leq 8$.

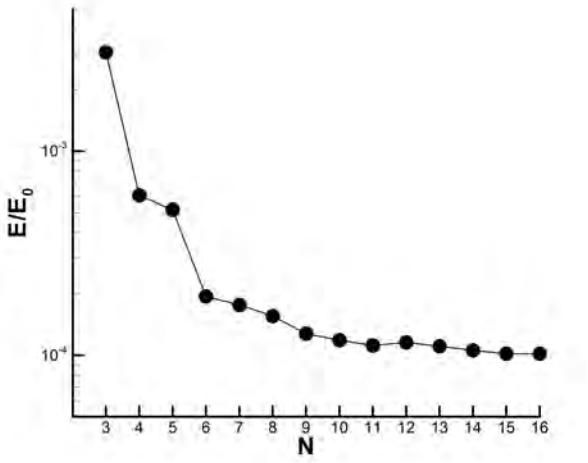

Figure 6: Energy ratio for toroids.

are symmetrical about $x = 0$. This explains the results for the separate components in Figure 8.

Figure 9 shows the scattered component of the free-surface elevation at $K = 1$ along radial lines at angles θ between zero and 90 degrees from the x-axis. Only one quadrant is shown since the real part is symmetric about $x = 0$ and the imaginary part is anti-symmetric. There is substantial angular variation of the elevation in the interior domain between the cylinder and torus. In the exterior domain outside the torus the elevation is relatively small, and attenuates rapidly with increasing radius as expected. The real part appears to be nearly axisymmetric. The amplitude of the scattered elevation for the cylinder alone is shown for comparison in the left-hand plot of Figure 9.

References

[1] Porter, R. 'Cloaking of a cylinder in waves,' IWWWFB26 (2011), Athens.

[2] Newman, J.N. 'Scattering by a cylinder with variable bathymetry,' IWWWFB27 (2012), Copenhagen.

[3] Bingham, H., (www.iwwwfb.org/Abstract/iwwwfb27/iwwwfb27_discussions.pdf, page 52)

[4] Newman, J.N., (www.wamit.com/Reports/2012ConsortiumReport.pdf, page 31)

[5] Farhat, M., Enoch, S., Guenneau, S. & Movchan, A.B. 'Broadband cylindrical acoustic cloak for linear surface waves in a fluid,' Physical Review Letters, **101**, 134501 (2008).

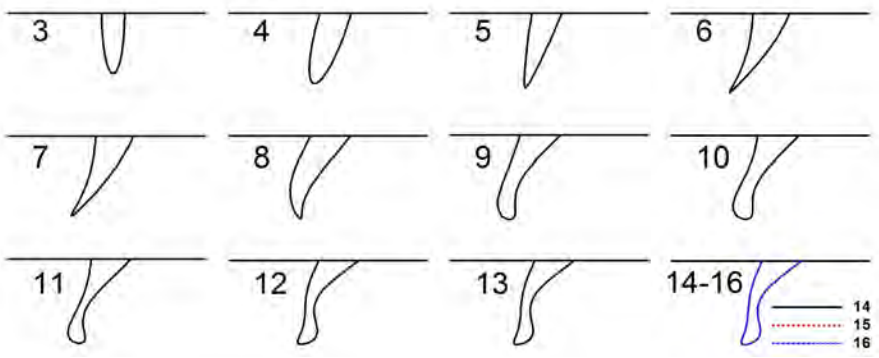

Figure 7: Cross-sections of the toroids. The sections $N = 14, 15, 16$ are superposed.

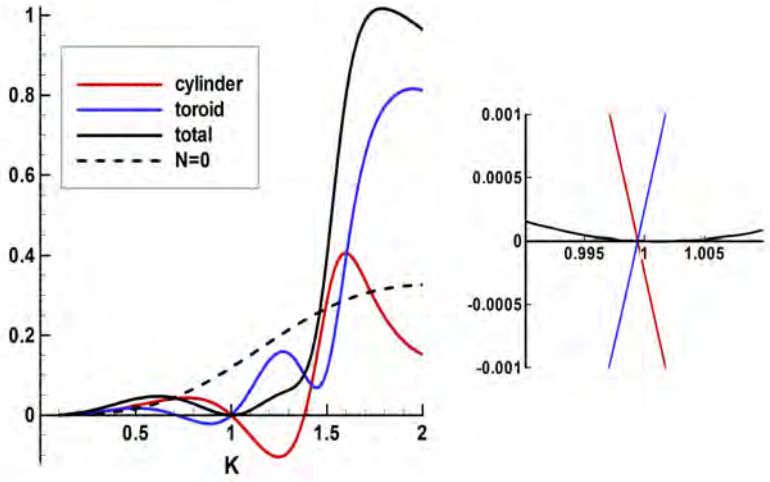

Figure 8: Total drift force on the configuration N=16 and separate components acting on the inner cylinder and toroid. The dashed line is the force on the inner cylinder alone (N=0). The small zoom figure on the right shows the zero-crossings of the components at K=1.

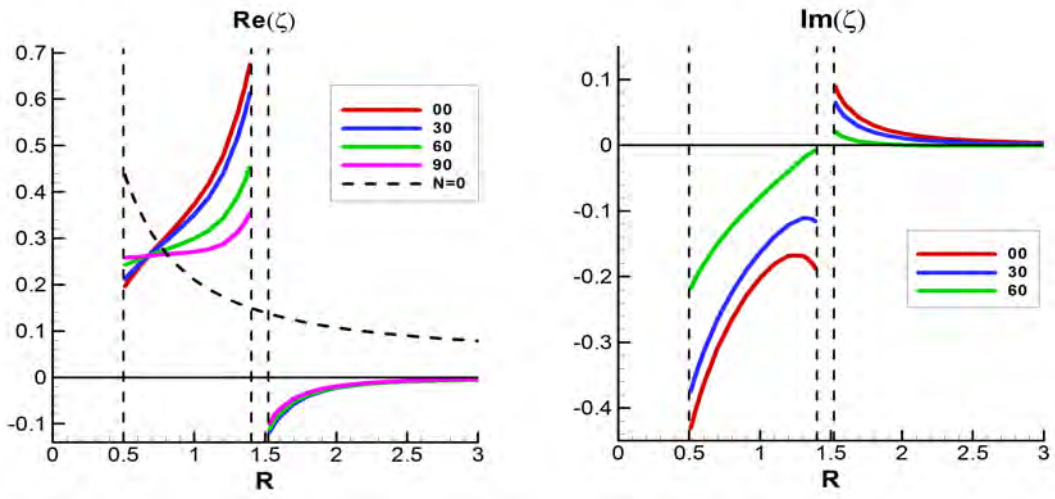

Figure 9: Real and imaginary parts of the free-surface elevation for the configuration N=16 at K=1, plotted vs the radius R at $\theta = (0, 30, 60, 90)$ degrees from the x-axis. The waterline radii of the bodies are indicated by vertical dashed lines. In the left-hand plot the line N=0 is the amplitude of the elevation for the cylinder alone, at θ=0.